Sustainable Microwave Assisted Synthesis And Anti-Proliferative Response of Starch-Based CNT-IO and CNT-ZO Nanocomposites: A Comparative Study

G. Deepthi Reddy
Palamuru University
M. Haseena
GITAM: Gandhi Institute of Technology and Management
M. Noorjahan
Palamuru University
A. Ratnamala
GITAM: Gandhi Institute of Technology and Management
Chandra Babu Naidu (chandrababu954@gmail.com)
GITAM Deemed To Be University-Bangalore

Research Article

Keywords: Tapioca sago, Hordeum vulgare, Eleusina coracona, CNT, Anti- proliferative, Anti-oxidant

Posted Date: November 15th, 2021

DOI: https://doi.org/10.21203/rs.3.rs-1045377/v1

Version of Record: A version of this preprint was published at Journal of Inorganic and Organometallic Polymers and Materials on March 1st, 2022. See the published version at https://doi.org/10.1007/s10904-022-02267-3.

Abstract

Starch based Carbon nanotubes-iron oxide (CNT-IO) and Carbon Nanotubes-Zirconium oxide (CNT-ZO) Nanocomposites (NCs) were fabricated by using facile microwave irradiation technique from different plant-based starch sources namely *Tapioca sago* (TS), *Hordeum vulgare* (HV) and *Eleusina coracona* (EC) and metal oxide precursor solutions. These NCs were studied using different characterization techniques such as SEM, TEM, XRD, Raman spectroscopy and FTIR spectroscopy. The Structural morphology of Starch based CNT-IO and CNT-ZO NCs observed like a rolled tubular structures and exhibiting strong blue luminescence with the charge transfer between CNT and Metal oxide. We have evaluated the anti-proliferative and anti-oxidant activity of starch-based CNT-IO and CNT-ZO NCs using MCF-7 cell line compared with the standard drug camptothecin and DPPH assay. Among the various NCs studied antiproliferative activity, CNT-IO and CNT-ZO obtained from starch source *Eleusina coracona* was effective with IC 50 values of 12.3 and 18.2 µg/mL respectively. Moreover, the enhanced radical scavenging activity has also been observed for these NCs.

Introduction

Green nanotechnology aids in the synthesis of eco-friendly, safe and commercially viable nano-technology based materials. The main objective of green technology plays a vital role in fabrication of materials that are safer. The electronic, photochemical, chemical and optical properties of metallic, carbon, polymeric and metal oxide based nanoparticles synthesized by green nanotechnology has been received attention rather than other materials [1]. The combination of nanoparticles by green technology, utilizing both biotechnology and nanotechnology, has gained much importance due to increasing need for the synthesis of customized and eco-friendly materials.

The exceptional and enhanced optoelectronic, catalytic, magnetic properties were exhibited by metal oxide nanomaterials in comparison to their counterparts [2, 3]. The noble metal nanoparticles are extensively studied as the free-electron excitations exhibits strong optical absorption in the visible region [4]. The novel zirconium and iron oxide metal nanoparticles are under high priority due to their numerous applications. These neoteric metal oxide nanoparticles are utilized in bio-labelling, optics (nonlinear), chemical reactions (catalyst), electric batteries to intercalate materials (optical receptors), anti-bacterial applications and selective spectral coating in absorption of solar energy.

It was earlier reported that different inorganic substrates like zeolites and silica were intrigued by metal carbon based nanoparticles, those displayed structure with core shell frames [5–7]. These materials were found to have important and effective attributes viz.., surface functionalization, photoelectric, physical and chemical characteristics which protects the species from tough unfavorable conditions with increased stability [8].

On the other hand, starch is eco-friendly, feasible, sustainable, polysaccharide [9, 10]. Plant based starch has complex coarse grained structures which are semi crystalline in nature. These crystals range from 1

– 100 mm in diameter [11]. Due to its undesirable characteristics like biodegradable and in toxic nature, starch is extensively used as drug carrier [12]. Application of metal oxide nanoparticles with starch polymers have attained great recognition for its ability of natural polymer shielding, thus increasing the forces to build up the consistency between different attractive forces acting on nanoparticles [13].

The advantages of microwave energy made them to utilize more in the studies for nanoparticle synthesis. The characteristic feature of homogenous heating is the most advantageous in using the energy source from microwave for producing specific nanoparticles. It was earlier reported that synthesis of iron oxide nanoparticles in compatible with organic materials using microwave method [14]. The synthesized iron oxide nanoparticles using microwave energy were utilized in the application of molecular imaging [15]. Mostly, hydrothermal technique was employed in synthesis of zirconia nanoparticles, often few reported, stated that nanoparticles of zirconia were synthesized using microwave method [16, 17].

The present work is focused on the development of new nanomaterials based on metal (Fe and Zr) oxides and carbon, where the soluble starch extracted from *Eleusina coracona* [EC], *Tapioca sago* [TS] and *Hordium vulgare* [HV] were used as the carbon sources. The nanomaterials were synthesized by microwave irradiation, which is very rapid and simple technique. The metal (Fe, Zr) oxide particles generated during the synthesis of nanoparticles were stabilized by the EC, TS and HV starch solution, which act as carbon source in this technique. The starch solution is mixed with the metal oxide precursor solution and the reaction mass obtained was further processed without the addition of any precipitating agent.

The synthesized materials were confirmed and characterized by XRD, Fourier transform infra-red spectroscopy (FT-IR), FT-Raman, scanning electron microscopy (SEM), Transmission electron microscopy (TEM),UV-Visible Spectroscopy and Photoluminescence Spectroscopy. MTT and DPPH assays were performed on MCF-7 cancer cell lines to analyze the cytotoxicity and the anti-oxidant activities of the synthesized NCs, respectively.

Experimental

2.1. Materials

Zirconyl Oxy Chloride ($ZrOCl_2.8H_2O$ 97%) was purchased from Fluka AG, Buchs SG, and Anhydrous Ferric Chloride ($FeCl_3$ 97%) was purchased from SDFCL, Mumbai, India and used without further purification. Tapioca sago(TS), Hordeum vulgare (HV) and Eleusina coracona(EC) grains were purchased from local supermarket. DMEM (Dulbecco's modified Eagles medium), MTT [3-(4,5-dimethylthiazol-2-yl)-2,5-diphenyl tetrazolium bromide], trypsin, EDTA, Phosphate Buffered Saline (PBS)were purchased from Sigma Chemicals Co. (St. Louis, MO) and Fetal Bovine Serum (FBS) was purchased from Gibco.25 cm 2 and 75 cm2 flask and 96 well plated purchased from Eppendorf India. Human breast cancer cell line MCF-7 was purchased from NCCS, Pune. DPPH (1,1-diphenyl-2-picryl hydrazyl) was purchased from Sisco Research Laboratories Pvt. Ltd., Maharashtra, India. All aqueous solutions were made using water (DW).

Microwave MW73V with 2450 MHZ MW output, made in Malaysia was used for the synthesis of nanocomposites.

2.2.Synthesis of CNT-Iron Oxide and CNT-Zirconia Oxide Nanocomposites

The starch sources from *Eleusina coracona* [EC], *Tapioca sago* [TS] and *Hordium vulgare* [HV] were employed in the synthesis of CNT-IO and CNT-ZO NCs with microwave method using anhydrous ferric chloride and Zirconyl oxy chloride as precursors. The seeds of EC, TS and HV purchased from the market were washed thoroughly with distilled water and dried in sunlight. The completely dried seeds of EC, TS and HV were finely powdered by grinding. These powders were used for the preparation of 5% (w/v) starch solutions, separately.

Six beakers with starch solutions (two with TS, two with HV and two with EC) were exposed to 800 W microwave energy for 10 min. Immediately, to the hot starch solutions of EC, TS and HV, added anhydrous $FeCl_3$ (2 g) to produce CNT-IO NCs and $ZrOCl_2.8H_2O$ (1.168 g) to produce CNT-ZO NCs separately, then exposed the beakers with mixture solutions to 800 W energy for other 10 min. in a microwave oven. The colloidal solutions are formed after the treatment. To the colloidal solutions, added ethanol and washed the solutions several times with distilled water. The washed colloidal solutions were incubated for 12 h for aging. After aging, the solutions were dried at 100°C for 24 h to obtain NCs. The NC powders produced consists of CNT-Iron oxide (IO) and CNT-Zirconia Oxide (ZO). The illustration scheme for Synthesis of CNT-IO and CNT-ZO NCs is shown in Figure.1.

2.3. Characterization

Structural Properties of NCs were thoroughly studied by using different characterization techniques. The particle size and crystalline phase of the LNM Fe_2O_3 particles were studied by X-ray diffraction (XRD) on X'pert Pro X-ray diffractometer (P analytical B.V., Netherlands) using Ni filtered Cu Kα radiation (λ = 1.5406) from 2θ = 0–60. The morphology of nanocomposites were investigated using ZEISS EVO 18 model Scanning Electron Microscopy, operating at 40 kV and a current of 30 mA at a scan rate of 0.388 min^{-1}. The Transmission Electron Microscopy (TEM) images of the nanocomposites were obtained on a JEOL JSM-6500F with an accelerating voltage of 200 kV to know the morphology. The chemical composition of designed nanocomposites were characterized by FTIR and spectroscopy using a Bruker Alpha FTIR spectrophotometer in order to know the organic moieties present in the sample using KBr pellet method (wavenumber range 800-3600 cm^{-1}) at room temperature.

2.4. In vitro Cytotoxicity of NCs

2.4.1.Cell Cultures

Human colon cancer cell line HCT-116, Human breast cancer cell line MCF-7 and Cervical cancer cell line HeLawere purchased from NCCS and the cells were maintained in DMEM (Dulbecco's modified Eagles medium), supplemented with 10% FBS, penicillin/streptomycin (0.5 mL^{-1}) at 37ºC in5%

CO_2incubator.Exposure studies with NZPs were conducted in MCF-7 cells seeded in culture grade flasks (T25 flasks, Tarson Inc., India).

2.4.2. Anti-proliferative activity of NCs using MTT Assay

To understand maximum efficacy of NCs, MTT assay was performed to assess cell metabolism, proliferation, and viability. Concisely, cells were seeded at 5×10^3cells density per well and incubated overnight in DMEM supplemented with 10% FBS at 37°C and 5% CO_2.next day, old media was discarded and replaced with 100µL of fresh media with different concentrations of NCs (5, 10, 25, 50,100 µg/mL) in 96 well plate and incubated for 48hours.Cells were incubated with fresh media with 100µL of MTT solution (0.5mg/mL^{-1}) for 3 h at 37°C in 5%CO_2 incubator. Cells with metabolically active mitochondria reduce MTT salt to chromophore formazan crystals which appears as precipitate in the 96 well plates. Camptothecin is used as a standard drug control. Microplate reader is used to read the optical density of solubilized crystals in DMSO at 570 nm. Average value of the optical density of the biological replicate standardized using negative control (cell culture medium and cells) and positive control (with drug) is used to determine Cell viability for each treatment group. All the experiments were performed in triplicates and IC50 was calculated from the graph thus attained

2.5. Anti-Oxidant activity of NCs

1,1-diphenyl-2-picryl hydrazyl (DPPH) assay was used to study antioxidant property, and potential to scavenge the free radicals. Reduction of ethanolic DPPH by a hydrogen donating antioxidant is the basis of the DPPH assay, DPPH is reduced to its non-radical form (DPPH-H). Current study uses 0.1mM DPPH solution prepared by dissolving 4 mg of DPPH in 100 ml of ethanol. Various concentration of NCs (50, 100, 150, 200 and250µg/mL) prepared using green technique was mixed with ethanol (40µL) and 3mL of DPPH solution (0.1mM) was added and incubated in dark at 37°C for 20min. UV-Vis spectrophotometer was used to record the absorbance of the test samples at 517nm.All the tests were performed in triplicate and percentage of inhibition values compared with standard reference compound (Ascorbic acid).

Radical Scavenging activity is calculated from the following formula.

% Radical Scavenging Activity (RSA) = [Abs (control) – Abs(sample) / Abs(control)] x 100

Results And Discussion

3.1. XRD Analysis

The X-ray diffraction analysis of starch-based CNT-IO and CNT-ZO NCs synthesized by microwave method disclosed the crystalline nature of the composites. In Figure .2(a) and (b), the crystalline peaks at $2\theta = 19.62^o$, 21.88^o, 26.29^o, 41.6^o were exhibited by the NCs in the X-ay diffraction analysis. The peak at 26.29^o corresponding to the graphitic (002) planes and the sharp peak at 41.6^o corresponds to (100)

planes of CNT. Moreover, improper alignment of CNT causes more defective structure [24, 25] due to the metal ion incorporation.

The nano sized carbon dots with CNT's were identified by the prominent peaks below 20^o and the later increased peak width was observed. In addition to the CNT peaks, in figure .2(a), IO is crystalline with the peaks at $2\theta = 30.2^o$, 33.4^o,35.2^0 40.86^o, 43.2^o,50.2^o,54.3^o and 62.4^o that were attributed to (220), (104), (311), (113), (400),(024),(116)and (440) lattice planes of the cubic and rhombohedral phases which corresponds to Maghamite (Y) and Hematite (α) phases, respectively [23, 26]. The results of CNT-IO NCs disclosed the reduced crystallinity nature in TS/CNT-IO compared to HV/CNT-IO and EC/CNT-IO i.e., the starch composite of TS/CNT-IO is less crystalline among the tested starch nanocomposites. In the process of conversion of starch to carbon dots and tubes, the formation of inverse spinel structure of iron oxide particles is crucial and is clearly distinguishable.

In Figure .2(b), the lattice (111), (200), (220), (311) and (211) planes of the tetragonal phase of ZO[27] produce the peaks at $2\theta = 30.5^o$,34.62^o, 50.58^o, 59.9^o and 61.9^o for CNT-ZO NCs, the peaks of composite ZO are slightly shifted when compared to the peaks of pure ZO synthesized by green technology [16]. The results and observations for CNT-ZO NCs revealed the reduced crystallinity nature in TS/CNT-ZO and HV/CNT-ZO compared to EC/CNT-ZO NCs. Thus the reduced crystallinity made the ZO more amorphous.

3.2. FTIR Analysis

The FTIR analysis revealed information about crystal morphology, nature of surface hydroxyl groups for starch based CNT-IO and CNT-ZO NCs(Figures 3(a) and (b)). Figure 3(a) corresponds to CNT-IO NCs and Figure 3(b) corresponds to CNT-ZO NCs. In both Figures 3(a) and (b)the characteristic FTIR peaks at 3416 cm^{-1}, 1650 cm^{-1}, 1470 cm^{-1}, 1034 cm^{-1} is due to the –OH stretching, -OH bending vibration ,CH stretching and CO stretching with respect to the carbon phase of starch solutions [32, 35, 36]. The additional peak at 584 cm^{-1} in figure 3 (a) confirms the Fe-O Stretching of deposited IO in the Carbon nanostructure [33] and the peaks at 2926 $cm^{-1}$and 600-800 cm^{-1} in figure 3 (b) confirms the CH stretching, Zr-O bonds in the carbon nanostructure [34].

3.3. FT-Raman Analysis

The Raman analysis is studied for starch-based CNT-IO and CNT-ZO NCs, shown in Figure .4(a) and (b). In XRD and FTIR analysis, the characteristic peaks of carbon material in the composites are not clearly defined, hence the Raman spectra reveals the nature of carbon component present in the composites. In both the figures 4(a) and (b),the corresponding Raman shift at ~1350 cm^{-1} and ~1580 cm^{-1} are characteristic D and G bands of carbon materials present in both the composites respectively [37, 38]. The characteristic peaks in figure. 4(a) at 200-290 cm^{-1},390 cm^{-1}, 590 cm^{-1} belongs to α-Fe_2O_3 and 500 cm^{-1} belongs to α/Y- Fe_2O_3 spinel structure confirms CNT-IO NCs[39]. In Figure .4(b) the peaks at 224 cm^{-1}, 292 cm^{-1}, 407 cm^{-1}, 636 cm^{-1} corresponds to tetragonal phase of Zirconia confirms CNT-ZO NCs[40].

3.4. UV-Visible spectra

The UV-visible spectrum of starch-based CNT-IO and CNT-ZO NCs at 200-1100 nm wavelengths were recorded and depicted in Figure 5(a) and (b). Prominent absorption bands at 321 nm, 360 nm, 408 nm, 500nm, 655 nm and 730 nm related to CNT-IO NCs were shown in the UV-visible spectra in figure 5(a). The charge transfer between O (2p) orbitals and Fe^{3+} (d) orbitals and the transitions in the ligand field of Fe^{3+} generated a strong absorption band at 321 nm in the UV-visible spectrum, whereas, the formation of ferric oxide nanoclusters with α and Y phases developed weak absorption bands at 360 nm, 408nm, 500 nm and 655 nm [28, 29]. Moreover, the formation of CNT-IO complex is due to the π →π* transition of π electrons in CNT, which is observed as a peak at 730 nm and is also confirmed by XRD analysis [30].

In figure 5(b), the UV-visible spectra showed that the CNT-ZO NCs has a prominent absorption band at 212 nm, 290 nm, 300-400 nm and 650-720 nm. The tetragonal Zirconia developed a characteristic blue peak, which is shifted from the bulk Zirconia to create a strong absorption band at 212 nm [31]. Further, the charge transfer from ligand to metal between O (2p) and Zr^{+4} (d) orbitals results in generation of absorption peak at 290 nm. Weak and broad absorption bands are observed at 300-400 nm and 650-720 nm which corresponds to Zr-O transitions and the formation of CNT-ZO complex due to π →π* transition of CNT π electrons, respectively [30]

3.5. Band Gap Energy

It is very essential to evaluate the material band gap for the nanomaterials, semiconductors. The distance between the conduction band and valence band of electrons is said to be band gap. It represents the minimum energy required for the electron in the valence band to excite to conduction band to participate in conduction. The energy required is known as band gap energy. Insulators possess large (>4 eV) band gap energy whereas it is low for semiconductors (<3 eV). The calculated band gap energies of CNT-IO and CNT-ZO NCs are tabulated in table 1. The band gap energies were calculated using the following formula mentioned below

$E_{bg}=1240/\lambda$ eV

Where E_{bg} corresponds to the band-gap energy and λ to the wavelength (nm) absorbed by the material

Table.1.Band gap calculated for Synthesized NCs

Sample	Absorbance (nm)	Band gap (eV)
TS/ CNT-IO	321, 360, 408, 500, 655, 730	3.86, 3.44, 3.03, 2.48, 1.89, 1.69
HV/CNT-IO	321, 360, 408, 500, 655, 730	3.86, 3.44, 3.03, 2.48, 1.89, 1.69
EC/ CNT-IO	321, 360, 408, 500, 655, 730	3.86, 3.44, 3.03, 2.48, 1.89, 1.69
TS/CNT-ZO	212, 290, 650	5.84, 4.27, 1.90
HV/CNT-ZO	212, 290, 700	5.84, 4.27, 1.77
EC/CNT-ZO	212, 290, 720	5.84, 4.27, 1.72

3.6. Photoluminescence spectra

The luminescence of pristine IO and ZO nanoparticles in the visible and UV regions were reported in our earlier papers [16, 26]. The intrinsic defects generated during the nanoparticle synthesis produces emission peaks in the visible region; moreover, the excitonic recombination generates an emission in the UV region. The surface passivation of the defects in the nanoparticle results in varied PL responses by the CNT matrix embedded with pristine IO and ZO nanoparticles. The increased luminescent properties exhibited by the defects in the CNT-metal oxide structures were studied experimentally and theoretically [41, 42]. Depending on the method of synthesis, defects in the surface and the morphology of the metal oxide (M-O), the emissions of the M-O may be reduced or intensified.

The high quality IO and ZO dots synthesized by green technology exhibited characteristic broad yellow-green, orange red emission (large defects, ionized oxygen vacancy) with a strong near band edge emission [16, 26]. On the other hand, in figure 6(a) and (b), the pl spectra recorded for CNT-IO and CNT-ZO NCs at 360 nm excitation wavelength showed the quenching effect showing lower order broad visible range emissions at 450 nm extending its tail to longer wavelength compared to sharp bands in pristine IO and ZO nanoparticles. These characteristic emissions may result due to reduction in the visible luminescence or replenishing the defects in the nanoparticles with CNT or the pristine IO and ZO transfers the photoexcited charges to CNT empty state orbitals. The enhanced reduction in the luminescence was more in CNT-IO and CNT-ZO NCs than pristine metal (Fe, Zr) oxide nanoparticles. In the process of IO and ZO nanoparticles synthesis with CNT network exhibited a strong blue emission and slightly green emission, generally produced by the concentration of CNTs and oxygen vacancies. In this synthesis, may be the sharp edges of pristine metal (Fe, Zr) oxide nanoparticles are connected to the CNT network.

3.7..SEM and TEM

Surface morphology and chemical composition of starch-based CNT-IO and CNT-ZO NCs were analyzed by scanning electron microscope equipped with energy-dispersive X-ray spectroscopy is shown in Figures. 7(a),(b). Present studies shows that IO and ZO particles with CNT frame work are observed as perfect dispersed spherical balls and rods under SEM analysis. The structures are of irregular

morphology, may be due to slight agglomeration of particles. EDAX analysis shows signal characteristics of Fe and O,Zr and O with incorporation of C without any impurity shown in Figures 7(e),(f) .

TEM is used to investigate the microstructure of starch-based CNT-IO and CNT-ZO NCs. Due to preferred heterogeneous nucleation and interfacial interactions, many IO and ZO nanocrystals on the CNTs are densely deposited.

The CNT has a rolled tube-like structure that can be seen clearly. The CNT plays a pivotal role in allowing IO and ZO nanoparticles to disperse on its surface, TEM image (Figure. 7 (c) and (d)), which depicts the lattice of both starch based CNT-IO and CNT-ZO NCs, reveals the close interfacial contact between CNT-IO and CNT-ZO .

3.8.Anti proliferative activity

Carbon nanotubes are known as modern tools in nano-biotechnology for their unique properties, have great potential applications in suitable substrates, cell growth in tissue engineering, biomedical devices, and as vectors for gene transfection [43, 44]. Daxiang Cui *et al*.,[45] who reported that the SWCNTs effect on HEK293 cells, cells were arrested in G_1 phase after 25 µg/ml exposure of SWCNTs in the medium, and this resulted in drastic decrement in the cell number in the S phase. Also Bottini *et al*.[46] showed the cytotoxicity effect of MWCNT carboxylic on T lymphocyte and T leukemia cells, which led to 50% cell death after 24 hours, with the use of TB. Tian *et al*. [47] showed that the effect of SWCNTs on cell viability of human keratinocytes at the concentration of 100 µg/ml gave 79, 50, and 31% viability after days one, three, and five, respectively, which correlates to our results. Another study has also reported functionalized CNT (hydroxylic (−OH) and carboxcylic (−COOH)) reduced cell viability to 33% with use of the MTT assay [48, 49].

In the present study, MCF-7(human breast cancer cell lines), were employed in assessing the cytotoxicity of starch-based CNT-IO and CNT-ZO NCs. Cytotoxic studies of pristine IO and ZO nanoparticles on MCF-7 cell lines were reported earlier in our previous papers [16, 26] showed good cell viability with IC_{50} values of 87.2 µg/ml and 59.70 µg/ml.IO and ZO nanoparticles with CNT conjugation dramatically reduced cytotoxicity compared to Pristine IO and ZO nanoparticles, may be related to decreasing probability in accessibility of Fe/Zr source with cells. The blocking of the entrance of CNT or the bonding sites of IO and ZO (generation of ROS) resulted in reduced toxicity. CNTs plays a crucial role in release of intracellular dissolved metal ions (that generate ROS) into cytosol, reach nucleus and results in the death of the cell.

Moreover, tracking studies revealed that the nucleus of MCF-7 cells contains CNT-IO and CNT-ZO NCs suggesting the effective deliver of target compounds into cytosol and nucleus of the MCF-7 cells.

In conclusion, the results indicated dose dependent cellular mitochondrial activity CNT-IO and CNT-ZO NCs shown in figures.8(a) and (b), where among all the CNT-IO and CNT-ZO NCs, EC/CNT-IO and EC/CNT-ZO NCs with less IC_{50} values of 0.488 and 0.936µg/ml could be used as diagnostic and therapeutic agent

for delivering the drug that facilitate the fluorescent bio-imaging and tracking compared to TS/CNT-IO, HV/CNT-IO, TS/CNT-ZO and HV/CNT-ZO NCs. Hence all the NCs have shown efficient antiproliferative activity with lesser IC_{50} values shown in table.2 might be due to the starting material is a bio material capped with metal ions inducing greater potential towards cancer cell death, opens a new avenue in biomedical applications.

Table.2.IC 50 values Synthesized NCs in Anti proliferative Activity

Sample	IC_{50} (µg/ml)
TS/CNT-IO	**1.080**
HV/CNT-IO	**1.301**
EC/ CNT-IO	**0.488**
TS/CNT-ZO	**1.165**
HV/CNT-ZO	**2.158**
EC/CNT-ZO	**0.936**

3.9. Antioxidant activity

The radical scavenging activity of starch-based CNT-IO and CNT-ZO NCssynthesized by microwave technique are depicted in Figures 9(a) and (b). The DPPH solution colour changed from deep violet to pale yellow gradually in presence of starch-based CNT-IO and CNT-ZO NCs. The low peak intensity of DPPH can be clearly visible from UV-Visible absorption curves. The free radical scavenging percentage was calculated from the absorbance decrease at 517 nm. The radical scavenging activity remains almost same with increase in the concentration of starch-based CNT-IO and CNT-ZO NCs. and compared with Ascorbic acid as standard antioxidant. The IC_{50} values are shown in the table. 3.

Table 3
IC 50 values Synthesized NCs in Anti oxidant Activity

Sample	IC_{50} (µg/ml)
TS/ CNT-IO	**45.597**
HV/CNT-IO	**22.109**
EC/ CNT-IO	**12.341**
TS/CNT-ZO	**46**
HV/CNT-ZO	**38.4**
EC/ CNT-ZO	**18.382**

Conclusions

Sustainable starch-based CNT-IO and CNT-ZO NCswere synthesized by simple and rapid microwave irradiation technique. Starch solutions of TS, HV and EC used as a carbon sources efficiently stabilizes the IO and ZO nano particles obtained during the treatment generated metal (Fe, Zr) Oxide-CNT frame work. The morphology of starch-based CNT-IO and CNT-ZO NCs were rolled tube like structures and exhibiting strong blue luminescence with the charge transfer between CNT and Metal oxide. Starch based CNT-IO and CNT-ZO NCs exhibited enhanced radical scavenging activity determined by DPPH assay. Among all CNT-IO and CNT-ZO NCs,EC/CNT-IO and EC/CNT-ZO NCs exhibited effective antioxidant activity with IC_{50} value of 12.3 and 18.2 µg/mL. The results suggest that EC/CNT-IO and EC/CNT-ZO NCs are most efficient in cytotoxicity againt MCF-7 cells. Hence, in the forthcoming years, starch based CNT-IO and CNT-ZO NCs by green technology using microwave technique may serve as cost effective and eco-friendly method for the synthesis and production of luminescent starch based carbon/metal (Fe, Zr) oxide composites in larger scale and acts as promising materials in bio imaging by tuning its luminescent properties.

Declarations

Acknowledgements

The authors are thankful to DST-INSPIRE-AORC, Delhi, INDIA for INSPIRE-SRF grant

References

1. N.K. P.Mohanpuria, S.K. Rana, Yadav, Biosynthesis of nanoparticles: technological concepts andfuture applications. J. Nanoparticle Res. **10**, 507–517 (2008)
2. A.P. Alivisatos, Semiconductor clusters nano crystals and quantum dots. Science **271**, 933–937 (1996)
3. V.L. Klimov, A.A. Mikhailovsky, Su Xu, A. Malko, J.A. Hollingsworth, C.A. Leatherdale, H.-J. Eiseler, M.G. Bawendi, Optical gain stimulated emission in nanocrystal quantum dots. Science **290**, 314–317 (2000)
4. M.B. Mohamed, V. Volkov, S. Link, M.A.E. Sayed, The ‘lightning’ gold nanorods: fluorescence enhancement of over a million compared to the gold metal, ChemPhysLett. 317 (2000)517–523
5. C.Hui,C.M.Shen, J.F.Tian,etal.,Core-shell Fe_3O_4@SiO_2 nanoparticles synthesized with well-dispersed hydrophilic Fe_3O_4 seeds. Nanoscale **3**, 701–705 (2011)
6. Q.Yue,J.L.Li, W.Luo,etal.,An interfacecoassemblyinbiliquidphase:toward core-shell magnetic mesoporous silica microspheres with tunable pore size. J. American Chem.Soc **137**, 13282–13289 (2015)

7. Y.H. Deng, C.H. Deng, D.W.Qi,etal.,Synthesisofcore/shellcolloidalmagnetic zeolite microspheresfortheimmobilizationoftrypsin. Adv.Mater. **21**, 1377–1382 (2009)
8. Z.K. Sun, X.R. Zhou,W.Luo,etal.,Interfacial engineering of magnetic particles with porous shells:towards magnetic core porous shell microparticles, NanoToday 11 464–482
9. D.R. Lu, C.M. Xiao, S.J.Xu,Starch-basedcompletelybiodegradablepolymer materials. Express Polym.Lett **3**, 366–375 (2009)
10. F.A. Aouada,L.H.C.Mattoso,E.Longo, Enhanced bulk and superficial Hydrophobicities of starch-, based bionanocomposites by addition of clay. Ind. Crops Prod **50**, 449–455 (2013)
11. A.Buléon, P.Colonna,V.Planchot,S.Ball,Starch granules:structure and biosynthesis. Int.J.Biol.Macromol **23**, 85–112 (1998)
12. D.K. Kim, M.Mikhaylova,F.H.Wang,etal.,Starch-coated superparamagnetic nanoparticles as MR contrast agents. Chem.Mater. **15**, 4343–4351 (2003)
13. W.Wu, Q.G.He, C.Z. Jiang,Magnetic iron oxide nanoparticles: synthesis and surface functionalization strategies. Nanoscale Res.Lett. **3**, 397–415 (2008)
14. I.F.Barahona,M.M.Hernado, F.Herranz, Microwave driven synthesis of Iron oxide nanoparticles for molecular imaging. Molecules. **24**, 1224 (2019)
15. E. Aivazoglou, E.Metaxa,E. Hristoforou Microwave assisted synthesis of IONP in biocompatible organic environment, AIP adv.8(2018)
16. G. Deepthi Reddy, M. Noorjahan, A. Ratnamala, M. Haseena, H. Manjunatha & K. Chandra Babu Naidu, Electrochemical characterization and biological applications of luminescent zirconia quantum dots,Applied Physics A 126(2020) 745.
17. K.P.S. S.Hembram, G.MohanRao, Microwave Synthesis of Zirconia Nanoparticles. J. Nannoscience and Nanotechnolgy **8**(8), 4159–4162 (2008),)()
18. S. Balajia, B.K. Mandala, S. Ranjan, N. Dasguptab, R. Chidambaram, **Nano-zirconia – Evaluation of its antioxidant and anticancer activity**, J. photochem. andPhotobiol. B: **170 (**2017**)125-133**
19. A. Miri, M. Sarani, Silver Nanoparticles: Cytotoxic and Apoptotic Activity On HT-29 and A549 Cell Lines. J.New.Dev.Che **4**, 10 (2018)
20. A.A. Kajani, A.K. Bordbar, S.H.Z. Esfahani, A.Razmjou, Green synthesis of anisotropic silver nanoparticles with potent anticancer activity using Taxusbaccata extract. RSC adv **00**, 1–12 (2016)
21. S. Soren, S. Kumar, S. Mishra, P.K. Jena, S.K. Verma, P.Parhi,Evaluation of antibacterial and antioxidant potential of the zinc oxide nanoparticles synthesized by aqueous and polyolmethod,Microb Pathog.119(2018) 145-151.
22. K. Chokshi, I. Panch, T. Ghosh, C. Paliwal, R. Maurya Arup Ghosh, S. Mishra, Green synthesis, characterization and antioxidant potential of silver nanoparticles biosynthesized from de-oiled biomass of thermotolerant oleaginous microalgae Acutodesmusdimorphus,RSC Adv. 6(2016) 72269-72274

23. M.V. Nosm, E.P. Etape, J.F. Tendo, B. V.Namond, P.T. Chongwain,et al., A Green and Facile Approach for Synthesis of Starch-Pectin Magnetite Nanoparticles and Application by Removal of Methylene Blue from Textile Effluent,J. Nanomaterials (2019) Article ID 4576135 12 pages
24. H. Soleimani, N.Yahya, M.K. Baig, L.Khodapanah,M.Sabet,M.Burda,A.OechsnerM. Awang, Synthesis of Carbon Nanotubes for Oil-water Interfacial Tension Reduction, Reduction,Oil Gas Res.1(1) (2015)
25. A.Cao,C.Xu, J.Liang,D.Wu,B.Wei, X-ray diffraction characterization on the alignment degree of carbon nanotubes. Chemical physics lett **344**, 13–17 (2001)
26. G. Deepthi Reddy, M. Noorjahan, A. Ratnamala, M. Haseena, H. Manjunatha & K. Chandra Babu Naidu, Meteoric synthesis of Luminescent Fe_2O_3 Nanoparticles: A potential Cytotoxic, Antioxidant & Bactericidal agent,InternationalJ.Applied Ceramic Tech.(2020).
27. Jung-M. Oh, S.K.O. Amar, Geiculescu, S.E. Creager, Mesoporous Carbon/Zirconia Composites: A Potential Route to Chemically Functionalized Electrically-Conductive Mesoporous Materials. Langmuir **28**, 3259–3270 (2012)
28. Y.P. He, Y.M. Miao, C.R. Li, S.Q. Wang, I. Cao, S.S. Xie, G.Z. Yang, B.S. Zou., Size and structure effect on optical transitions of iron oxide nanocrystals. Phys.Rev. **71**, 125411–125419 (2005)
29. G.M. Sulaiman, A.T. Tawfeeq, A.S. Naji, Biosynthesis, characterization of magnetic iron oxide nanoparticles and evaluations of the cytotoxicity and DNA damage of human breast carcinoma cell lines,Artificial cells, nanomed and biotech. 46(6)(2018) 1215
30. D. A.Lakshmi, M. Lydia Gracelin, Vigneshwari, P. Karpagavinayagam V. Veeraputhiran, C. Vedhi, Microwave Synthesis and Characterization of Multiwalled Carbon Nanotubes (MWCNT) and Metal Oxide Doped MWCNT. J.Nanoscience and Tech. **1**(1), 19–22 (2015)
31. Y. Kuthati, R.K. Kankala, S.X. Lin, C.F. Weng, C.H. Lee,, pH-Triggered Controllable Release of Silver-Indole-3 Acetic Acid Complexes from Mesoporous Silica Nanoparticles (IBN-4) for Effectively Killing Malignant Bacteria. Mol. Pharma **12**, 2289–2304 (2015)
32. C.Anyika,N.A.Md.Asri,Z.A.Majid,A.Yahya,**J.Jafaar**, **Synthesis and characterization of magnetic activated carbon developed from palm kernel shells,Nanotechnol**. Environ. Eng. 2(**16**) **(**2017**)**
33. M. Zahoor, F.Ali khan, Adsorption of aflatoxin B1 on magnetic carbon nanocomposites prepared from bagasse. Arabian J. Chemistry (2014). DOI:10.1016/j.arabjc.2014.08.025
34. S.Yakout, H.Hassan, Adsorption Characteristics of Sol Gel-Derived Zirconia for Cesium Ions from Aqueous Solutions. Molecules **19**(7), 9160–9172 (2014)
35. C.Saikia,A.Hussain,A.Ramteke,H.K.Sharma,T.K.Maji,Cross linked thiolated starch coated Fe_3O_4 magnetic nanoparticles:effect of montmorillonite and cross linking density on drug delivery properties,Starch/Stärke 66(2014)760–771
36. S.Palanikumar,B.Meenarathi,L.Kannammal,R.Anbarasan,Synthesis, characterization and catalytic activity of furosemide-functionalized ferrite on the sedimentation behavior of starch,Appl.Nanosci.5(2015)83–91

37. K. Song, Y. Lee, M.R. Jo, K.M. Nam, Y.M. Kang, Comprehensive design of carbon encapsulated Fe3O4 nanocrystals and their lithium storage properties. Nanotechnology **23**, 505401 (6pp) (2012)
38. E. Mohameda, M. Taheria, M. Mehrjoob, M. Mazaheric,n, A.M. Zahedia, M.A. Shokrgozarb, F. Golestani-Fard, In vitro biocompatibility and ageing of 3Y-TZP/CNTs composites, Ceramics International 41(10) Part A (2015) 12773-12781
39. M.J. Jesica, Santillan, D.M.Arboleda, D.F., M.B. Coral, D. Fernandez van Raap, D.C. Muraca, Schinca et al., Optical and Magnetic Properties of Fe Nanoparticles Fabricated by Femto second Laser Ablation in Organic and Inorganic Solvents. Chem.Phys.Chem **18**, 1192–1209 (2017)
40. S.N. Basahel, T.T. Ali Mohamed, M.K. Narasimharao, Influence of crystal structure of nanosized ZrO2 on photocatalytic degradation of methyl orange. Nanoscale Research Lett **10**, 73 (2015)
41. Y.H. Lu, Z.X. Hong, Y.P. Feng, S.P. Russo, Roles of carbon in light emission of ZnO,Applied Physics Lett. 96 (9)(2010) I.D. Article 091914
42. Y. Hu, H.-J. Chen, Enhancement of green luminescence of ZnO powders by annealing with carbon black. Mater. Res. Bull. **43**(8-9), 2153–2159 (2008)
43. D.Zhang,C.Yi,J., ,Y. Zhang, ,X. Chen, ,M. Yao, Yang, The effects of carbon nanotubes on the proliferation and differentiation of primary osteoblasts. Nanotech **18**, 475102 (2007)
44. U.C.Tam X.Chen, J.L. Czlapinski, G.S. Lee, D. Rabuka ,A. Zettl, et al.,Interfacing carbon nanotubes with living cells, J. American Chem. Soc. 128 (2006)6292–3
45. F. D.Cui, ,C.S. Tian, M. Ozkan, ,H. Wang, Gao,Effect of single wall carbon nanotubes on human HEK293 cells,Toxicollett. 155(2005)73–85
46. S. M.Bottini, ,K. Bruckner, N. Nika, S. Bottini, Bellucci ,A. Magrini, et al.,Multi-walled carbon nanotubes induce T lymphocyte apoptosis,ToxicolLett. 160(2006)121–6
47. F. Tian, D. Cui, ,H. Schwarz ,GG. Estrada, H. Kobayashi,Cytotoxicity of single-wall carbon nanotubes on human fibroblasts. Toxicol *in vitro* **20**, 1202–1212 (2006)
48. S. A.Magrez, ,V. Kasas, ,N. Salicio, W. Pasquier ,J, M. Seo, Celio et al., Cellular toxicity of carbon-based nanomaterials. Nano Lett. **6**, 1121–1125 (2006)
49. P. P.Wick, K. Manser L, ,U. Limbach, ,F. Dettlaff-Weglikowska, Krumeich ,S. Roth et al., The degree and kind of agglomeration affect carbon nanotube cytotoxicity. Toxicol. Lett. **168**, 121–131 (2007)

Figures

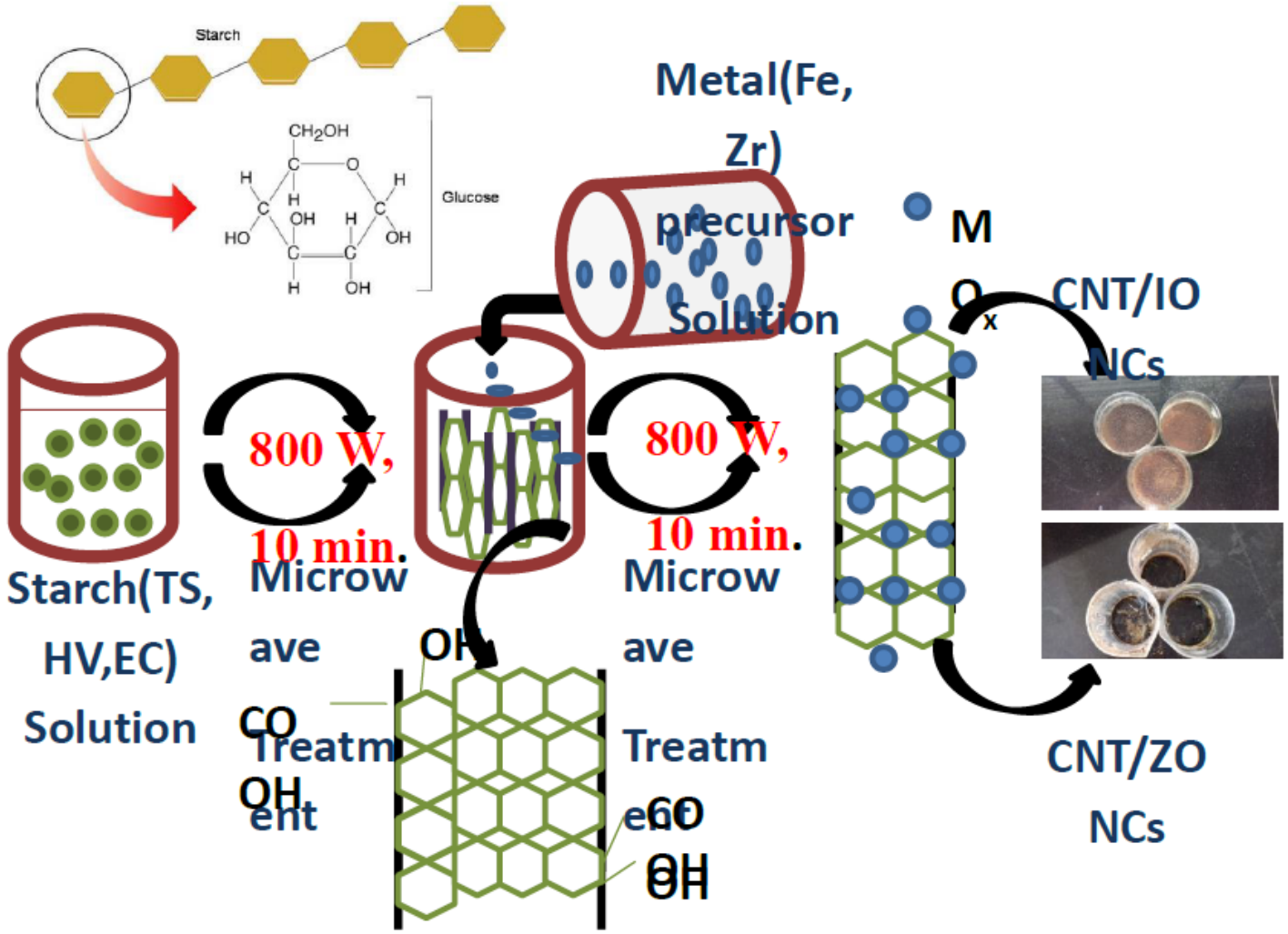

Figure 1

Illustration scheme for synthesis of starch-based CNT-IO and CNT-ZO NCs

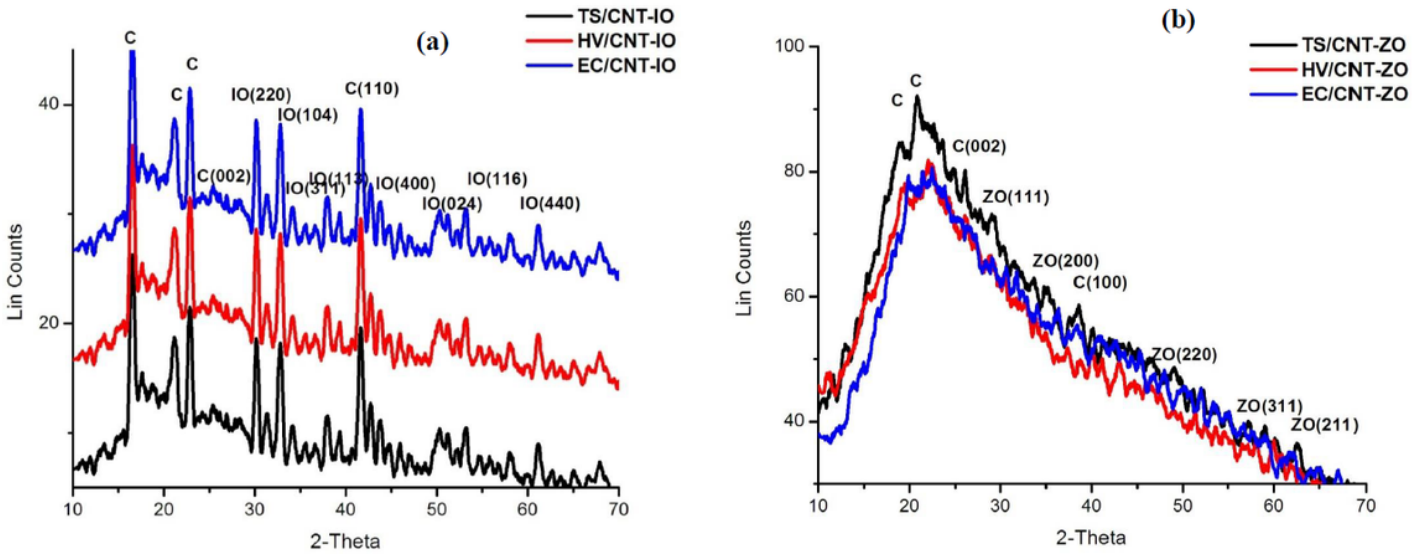

Figure 2

XRD Analysis of NCs a)CNT-IO NCs b)CNT-ZO NCs

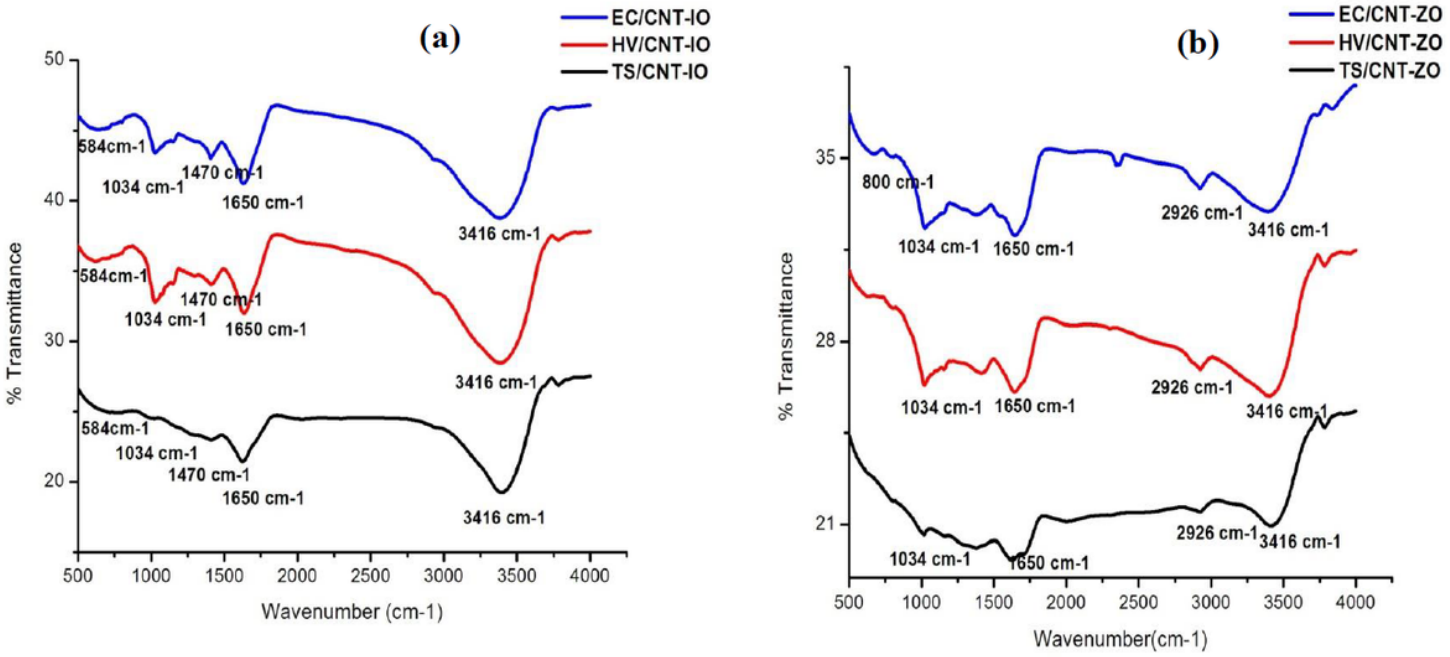

Figure 3

FTIR Analysis of NCs a)CNT-IO NCs b)CNT-ZO NCs

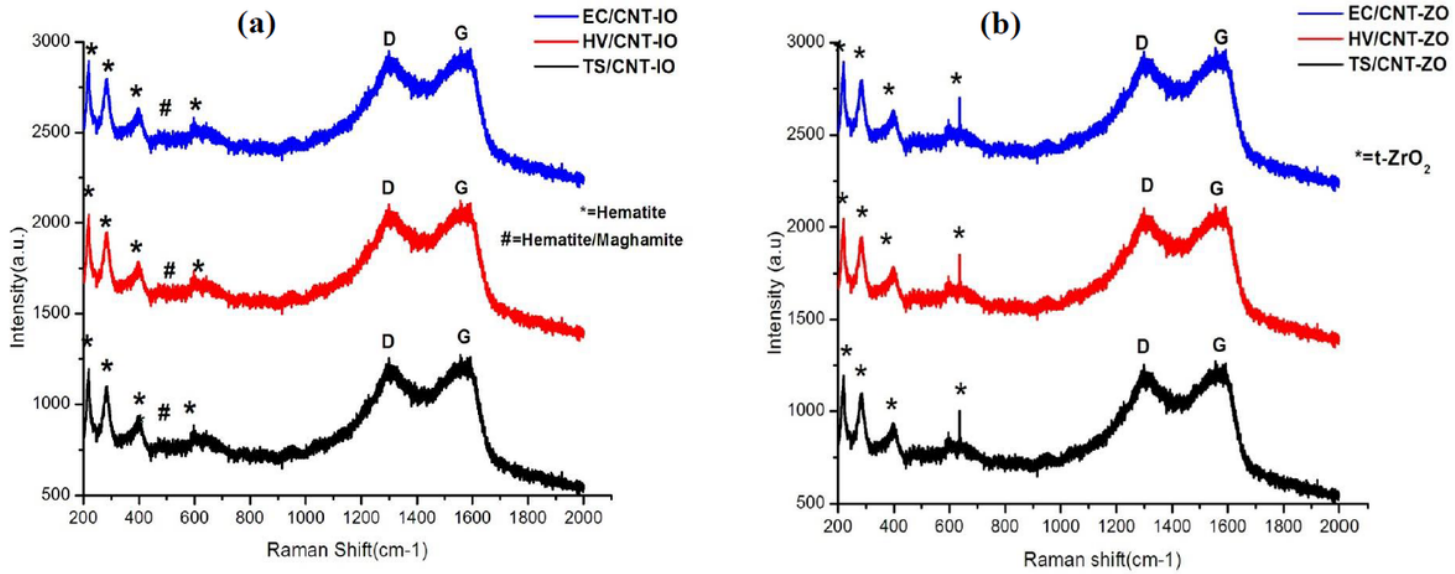

Figure 4

FT-Raman Analysis of NCs a)CNT-IO NCs b)CNT-ZO NCs

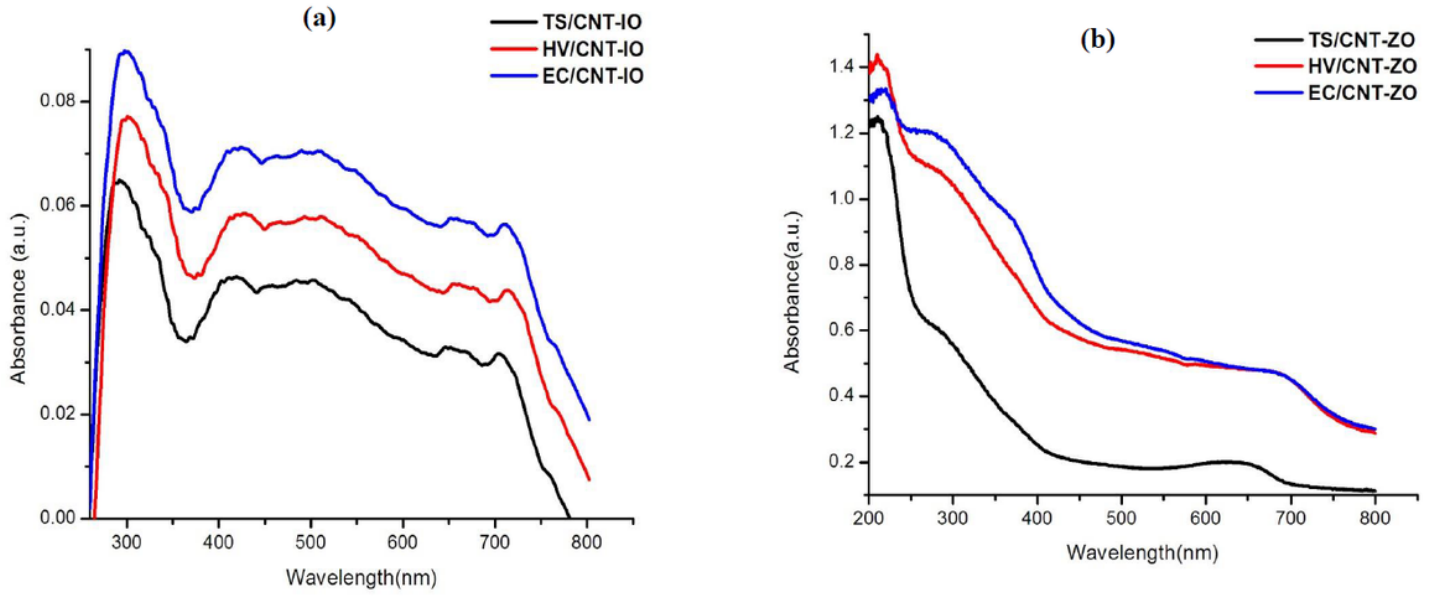

Figure 5

UV-VIS spectra of NCs a)CNT-IO NCs b)CNT-ZO NCs

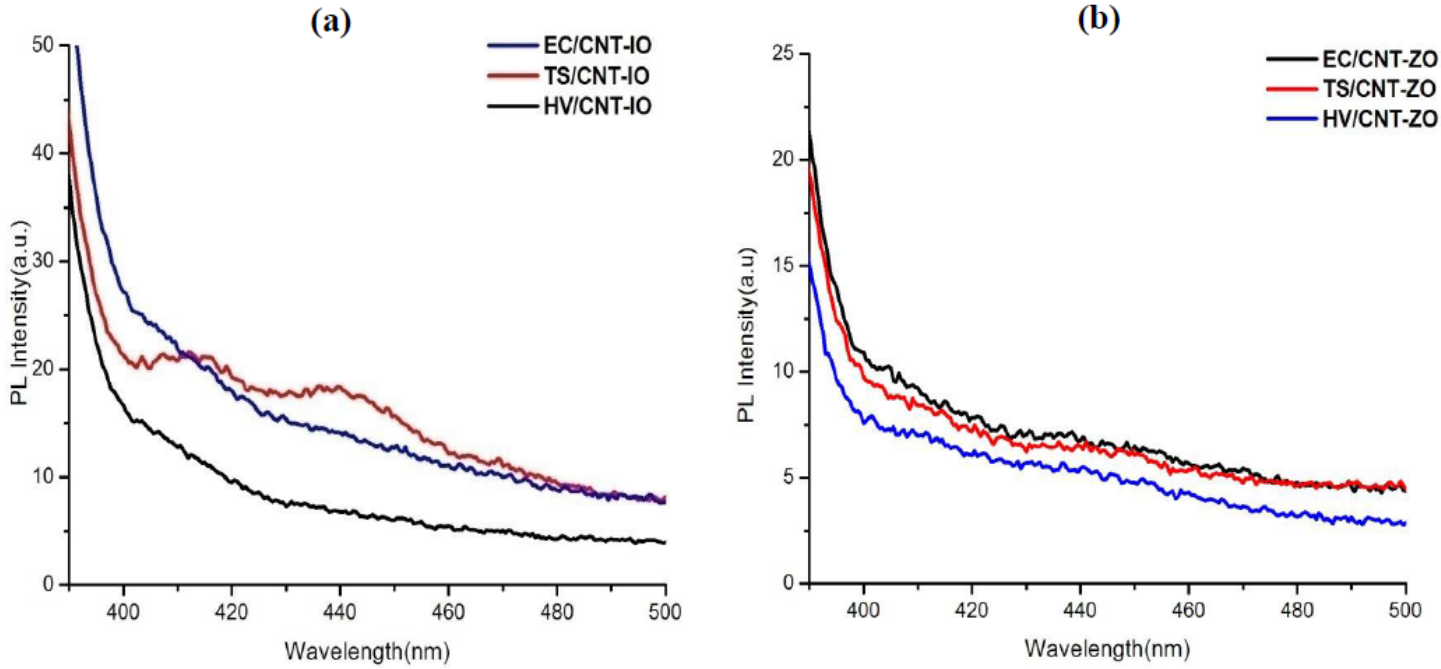

Figure 6

Emission spectra of NCs a)CNT-IO NCs b)CNT-ZO NCs

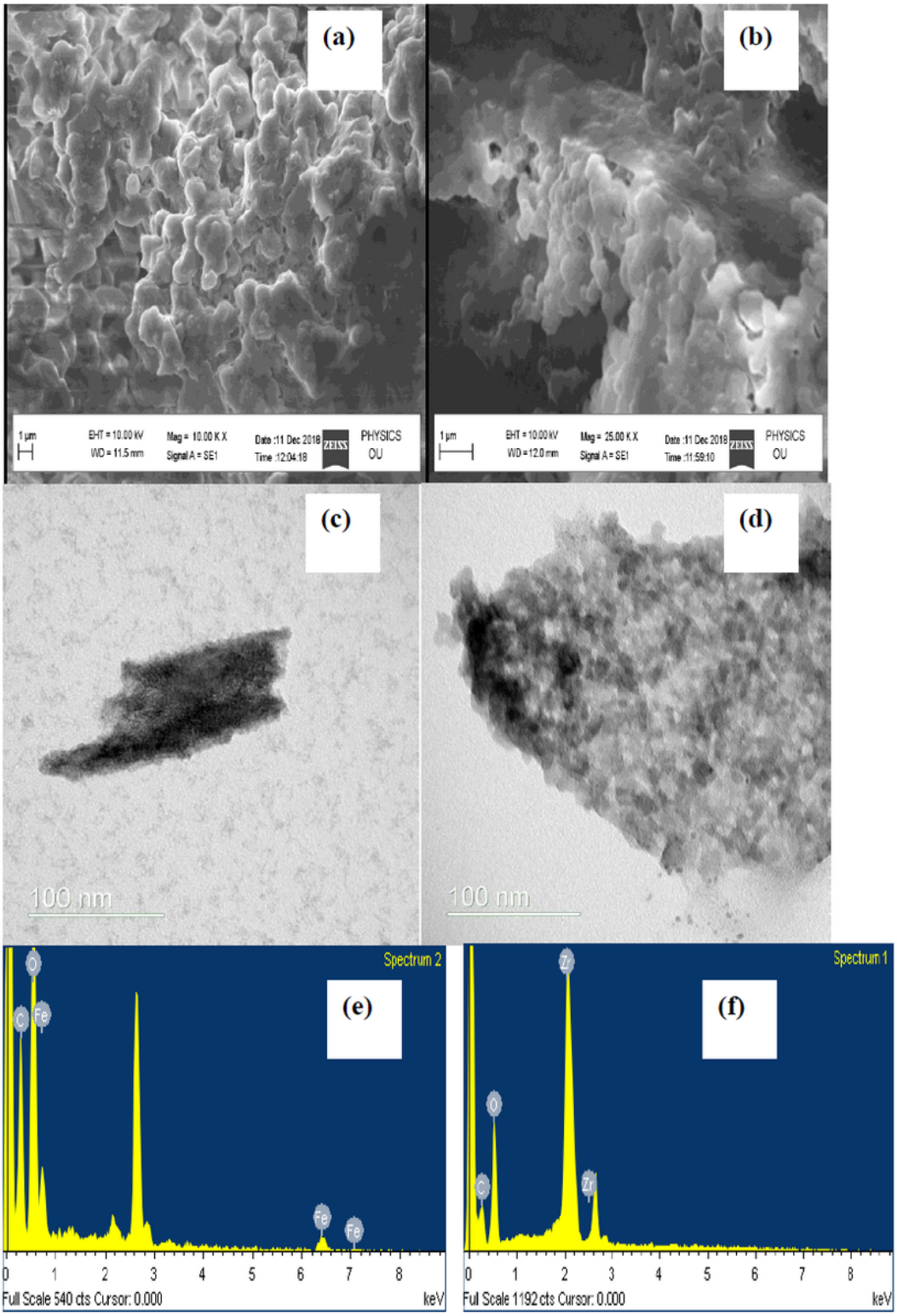

Figure 7

SEM and TEM of NCs

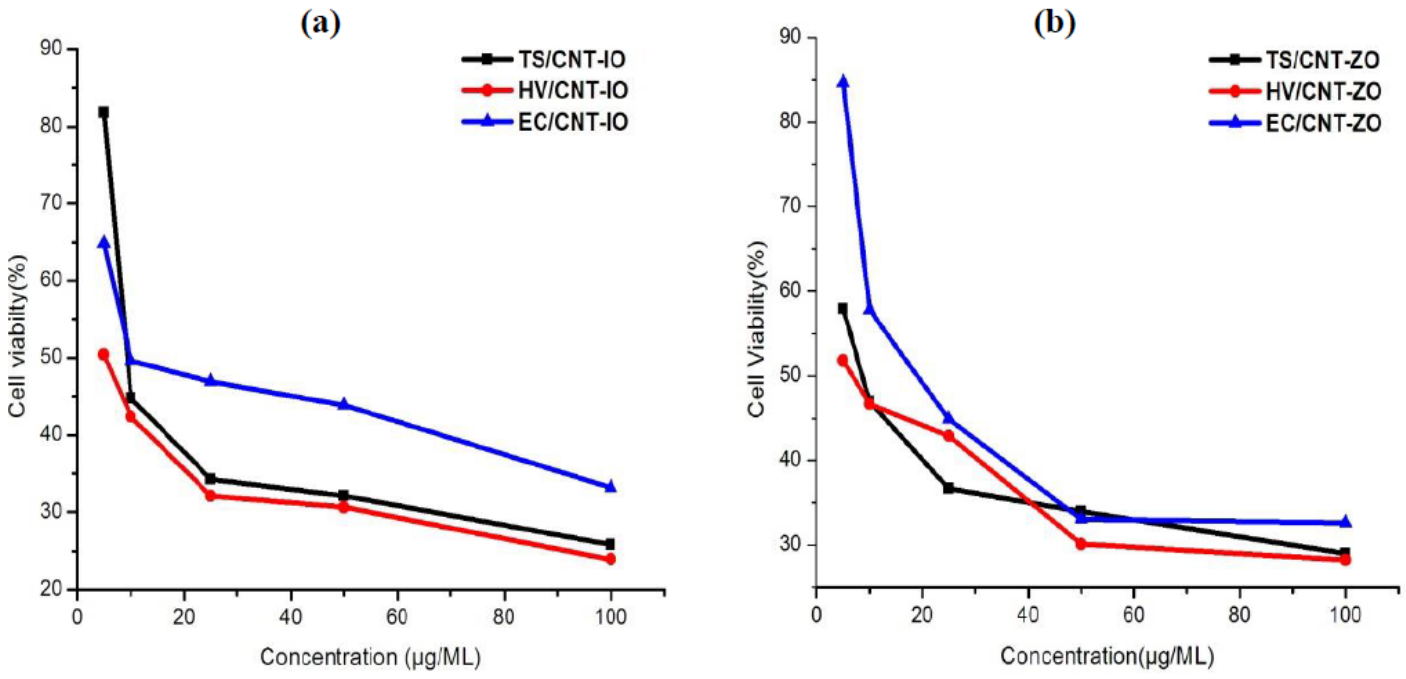

Figure 8

% Cell Viability of NCs a)CNT-IO NCs b)CNT-ZO NCs

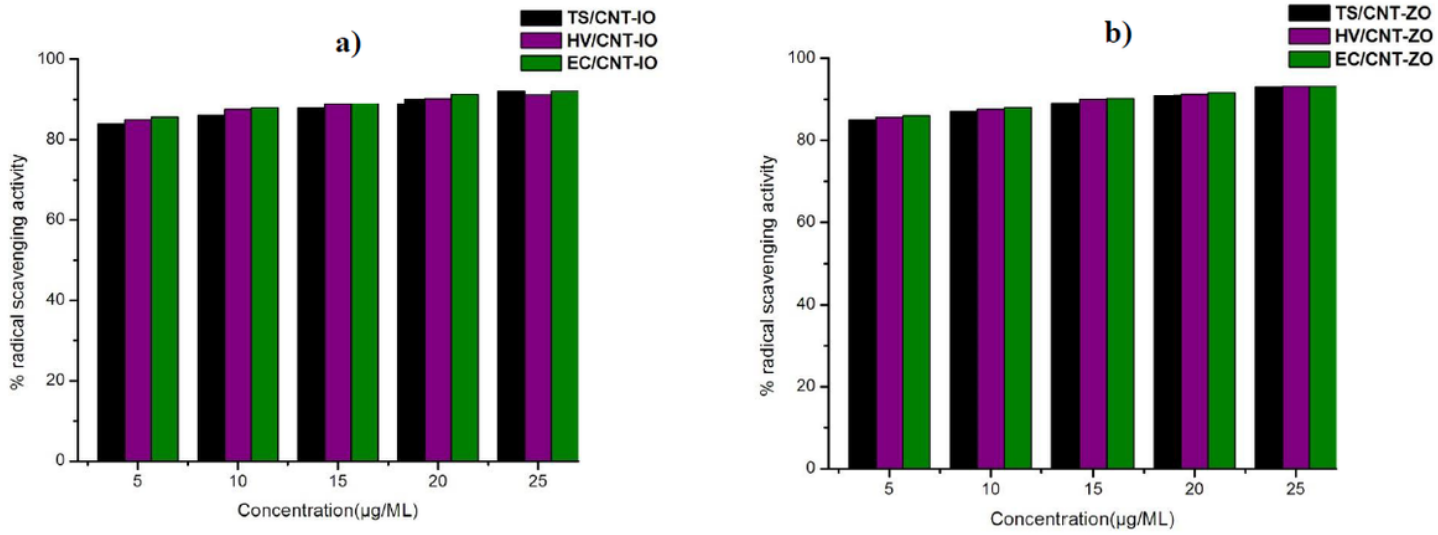

Figure 9

% Radical Scavenging activity of NCs a)CNT-IO NCs b)CNT-ZO NCs